Gerrid Brockmann, Anne Hartmann, Martin Kriegel

Validation of Simulated Velocity Distribution in Isothermal Mixing Ventilation Cases with Particle Streak Tracking

Submitted to *International Journal of Indoor Environment and Health* (Wiley)

Gerrid Brockmann, Anne Hartmann, Martin Kriegel

Validation of Simulated Velocity Distribution in Isothermal Mixing Ventilation Cases with Particle Streak Tracking

March 7, 2022

Hermann-Rietschel-Institut
Fachgebiet Energie, Komfort & Gesundheit in Gebäuden
Marchstr. 4
D-10587 Berlin

Prof. Dr.-Ing. Martin Kriegel
Telefon: +49-(0)30-314 24170
Fax: +49-(0)30-314 21141
E-Mail: kontakt@tu-berlin.de

Homepage: http://www.hri.tu-berlin.de

Abstract

Keywords: airflow characteristic, airflow structure, turbulence models, computational fluid dynamics (CFD), experimental fluid dynamics (EFD)

This is a validation study for the velocity distribution in mixing ventilation. Two different supply air diffusers a slot and a swirl diffuser form two different room airflows. For the swirl diffuser two different and for the slot diffuser five different exhaust positionings are tested numerically and experimentally. A comparison of the flow structure shows good agreement between simulation and experiment for six air changes per hour, but not for the lower air change rate of 1.5 per hour. The velocity deviations between experiment and simulation are higher for the swirl diffuser. These exist partly due to the experimental methodology, but also due to an overestimation of the supply air momentum. Thus further sensitivity investigations are carried out for the swirl diffuser. The overestimation of the supply air momentum depends mainly on an geometric model error in the CFD simulation. A comparison of different turbulence models confirms the advantages of the RST elliptic blending turbulence model over the k-epsilon realizable model for the swirl diffuser case.

Nomenclature

Acronyms

Acronym	Meaning
CFD	computational fluid dynamics
EFD	experimental fluid dynamics
PST	Particle-Streak-Tracking
RANS	Reynolds-averaged Navier–Stokes
RST	Reynolds Stress Transport

Symbols

Symbol	Unit	Meaning
α	$^\circ$	angle
Ar		Archimedes number
n	h^{-1}	air change rate
Q	$\mathrm{m}^3\,\mathrm{h}^{-1}$	volume flow rate
Sim'		similarity of the vector directions
Sim''		similarity of the vector magnitudes
T	K	temperature
τ	min	age of air
u	$\mathrm{m}\,\mathrm{s}^{-1}$	velocity

Indices

Index	Meaning
bz	breathing zone
ea	exhaust air
exp	experimental
i	generell index
num	numerical
sa	supply air

1 Introduction

This validation study is part of a research project about the influence of the exhaust positioning on the ventilation effectiveness. In addition, there are uncertainties about the influence on the airflow structure in the room. In general, the room airflow is expected to be characterized by the supply air position, orientation and velocity and remains unaffected by the exhaust air diffuser. This can be explained by the fact that the airflow near the exhaust opening assumes a potential flow without depth effect [1]. Kandzia [2] found out that there are "unstable" mixed ventilation structures in which a structure change is observed due to the change of the exhaust air position. For this purpose a computational fluid dynamics (CFD) parameter study should be executed. CFD has the advantage to get a full view over the room parameters and it is much faster and cheaper to achieve data. The accuracy of numerical data "depends greatly on user experience, the available validation data, and the effort made to verify solutions" [3]. Thus, a comparison of the numerically gained data with other approaches is mandatory. The ASME [4], Chen and Srebic [5] and Coleman et al. [6] provide standards for verification and validation in CFD and heat transfer.

Focus in this study is on the comparison of the velocity distribution for chosen isothermal test cases. The numerical data is a RANS based CFD-Simulation and the experimental fluid dynamics (EFD) data is measured with Particle-Streak-Tracking (PST) [7] and omnidirectional hot-wire anemometry. With the help of a PST system, two-dimensional velocity fields can be tracked over a relatively large spatial cross-section and accordingly offers a significantly high data depth. The individual measured anemometer spots serve twofold: they have a wider range to track velocities out of the range of the PST system and they can evaluate the tracked velocity magnitude. As requested by Oberkampf and Barone [8] for proper validation, the velocity vectors are determined experimentally so that not only a qualitative image matching but also a quantitative evaluation of the similarity of simulation and experiment is performed.

The evaluation of the similarity takes place on the one hand regarding the direction

of the vectors and on the other hand regarding the velocity magnitude. As a similarity measure for the direction of vectors the cosine theorem [9, 10] will be used. Generally, deviations between experiment and simulation are to be expected. In the case of measurements, the error is determined above all by the accuracy of the measurement technology, the tightness of the test chamber and the ducts. In the CFD simulation, there are the numerical errors, input uncertainties and physical model uncertainties [11]. The numerical error tells how well the underlying equations are solved: verification [12]. The model error indicates how well reality is described: validation. This error has to be determined.

To quantify the input uncertainty or to derive improvements to the model, if necessary, the geometric sizes of the modeled swirl diffuser and the cross-section of the exhaust diffusers are varied for one scenario. Finally, different turbulence models are compared with each other.

2 Methods

2.1 Geometry

Figure 1 shows the test stand. The test stand is located in the air-conditioned experimental hall of the Hermann-Rietschel-Institut. The floor area is 5.2 m x 4.4 m and the room height is 2.9 m. A glass front on one side of the experimental room offers the possibility to observe and visualize the experiments. Five exhaust air positions allow different exhaust air scenarios. Each exhaust position consists of three ventilation valve diffusers[1], each has the same distance (approx. 1.2 m) from each other. In the left half of the room on the ceiling is the first exhaust air diffuser ea1 with 0.2 m distance from the exhaust center to the left wall. Mirrored on the right half of the ceiling there is ea2. In the right half of the room, at a height of 0.2 m from the floor, is the exhaust diffuser ea3. The exhaust air positions ea4 and ea5 are located on the left wall at a height of 0.2 m and 2.5 m from the floor. Each exhaust position has a fully closable volume flow controller and allows a balancing of the volume flows or a forced volume flow ratio when several diffusers are used at the same time. Thus, different test cases can be investigated. The air sucked through all open exhaust air positions is merged and transported by a fan, which is placed on top of the test stand. The total volume flow is determined with a flow measurement via an orifice plate in front of the fan and adjusted by controlling the fan speed. The supply air is introduced through the central swirl diffuser[2]. Alternately, the supply air can be provided at the left wall through slot diffusers[3] installed at a height of 2.8 m. The supply air is preconditioned by a mobile HVAC-system [13]. With this mechanical ventilation system air exchange rates between 1 and 10 h^{-1} are possible to generate. The air is drawn from the experimental hall (the ambient air of the test stand). The hall uses a mixing ventilation scheme and the exhaust air temperature is regulated to a constant level of 20.4 °C.

[1] Trox GmbH, LVS/125/G1/P1-RAL9005-70%
[2] Trox GmbH, VDW-Q-Z-V/500x24/P1-RAL9005-70%
[3] Trox GmbH, VSD35-1-AK-M-L/600x98/C1/P1-RAL9005-70%

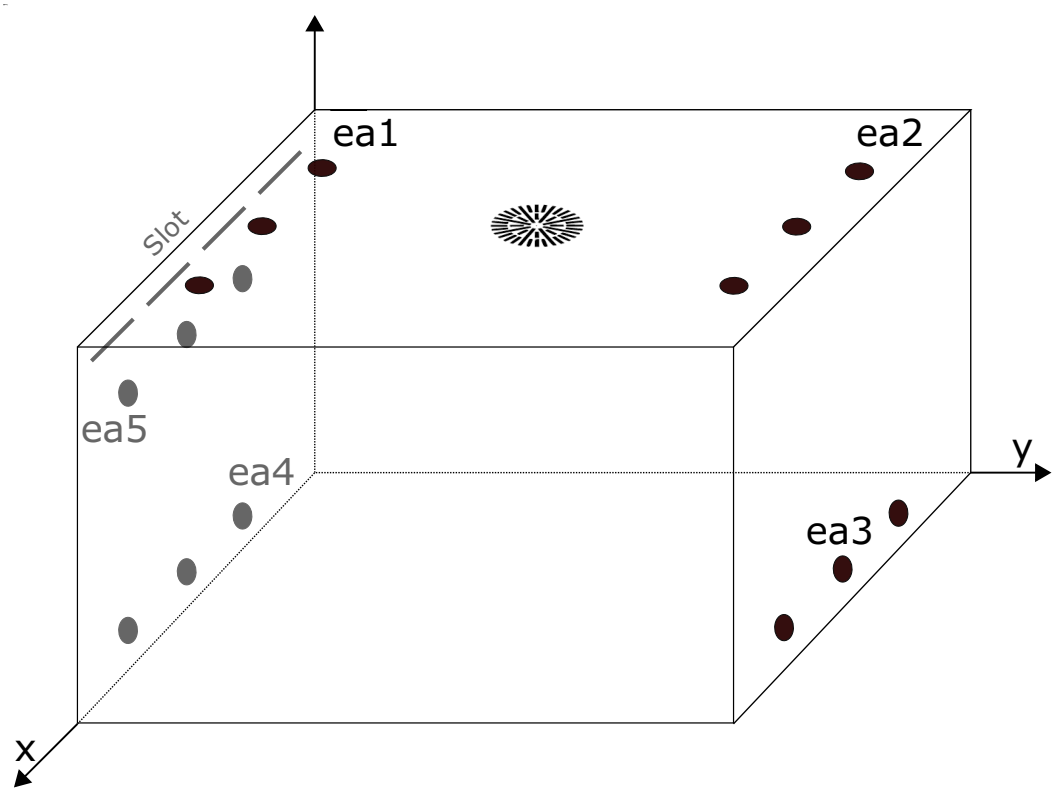

Figure 1: Design of the test stand with a slot and a swirl supply air diffuser and five exhaust positions (ea1 to ea5)

2.2 Parameter Setups

Different parameter setups are chosen (see Table 4). There are two supply air (sa) possibilities: slot or swirl diffuser. For the swirl diffuser the exhaust air (ea) openings ea1 and ea2 at the ceiling (ea12) or the openings ea3 and ea4 at the bottom (ea34) are open. For the slot diffuser all openings ea1 till ea5 are tested individually. The air change rate parameters n are 1.5 or 6 per hour.

Table 4: Summary of all measured cases

case	sa	ea	$n\,(1/h)$
ea12.i3	swirl	12	1.5
ea12.i5	swirl	12	6
ea34.i3	swirl	34	1.5
ea34.i5	swirl	34	6
ea1.i3	slot	1	1.5
ea1.i5	slot	1	6
ea2.i3	slot	2	1.5
ea2.i5	slot	2	6
ea3.i3	slot	3	1.5
ea3.i5	slot	3	6
ea4.i3	slot	4	1.5
ea4.i5	slot	4	6
ea5.i3	slot	5	1.5
ea5.i5	slot	5	6

2.3 Measuring Velocity Distribution

The visualization of the room airflow is performed by a PST system. The system is a fast measurement method for two-dimensional velocity measurements of room airflows in one plane and based on the investigations of Müller et al. [14, 7, 15]. Figure 2 shows a snapshot of the installed experiment.

The light-sectioning system is constructed from freely movable optics and is illuminated according to a predetermined pattern (short-pause-long). With the help of a bubble generator[4], small bubbles filled with a helium-air mixture are generated [16]. These bubbles follow the airflow, as their density is almost the same as room air. After capturing the moving bubble tracks with a high-resolution digital camera[5], the images are analyzed using image processing software ImageJ[6]. The pairs of tracks of double-exposed tracer particles on one taken picture are searched by the program considering the given suitability criteria. Knowing the track distance and pulse time the velocities are determined.

For the swirl diffuser setup only one camera position is used to track the area of

[4]Developed und manufactured by the Hermann-Rietschel-Institut, Technische Universität Berlin
[5]CANON EOS 5D
[6]National Institutes of Health

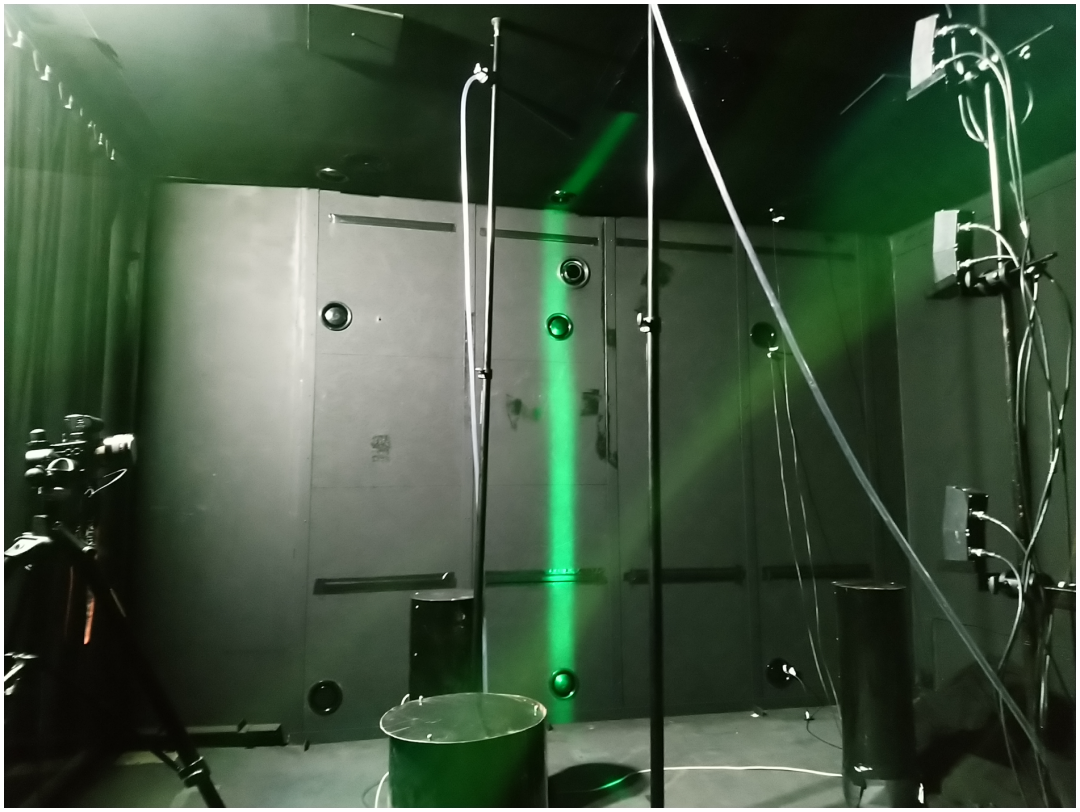

Figure 2: Snapshot of a PST measurement: The light section spans a plane from the center of the room to the exhaust air diffusers ea1, ea4, ea5. The camera is possitioned ortogonally.

interest (see Figure 3a). For the slot diffuser three different camera positions are merged to match the hole room section (see Figure 3a). A fourth camera position is used to track the higher velocities in the supply air zone with a adapted frequency. 30 pictures are taken for every set up and position. The resulting vector data is combined to one csv-file.

Additionally, a system of omnidirectional hotwire anemometer, Dantec Comfort Sense[7] is used to measure the velocity at a few points to get precise information about the velocity magnitude in the occupation zone and in the supply air zone.

[7]Dantec Dynamics, accuracy: ±2 % for 0 - 1 $\mathrm{m\,s^{-1}}$, ±5 % for 1 - 5 $\mathrm{m\,s^{-1}}$

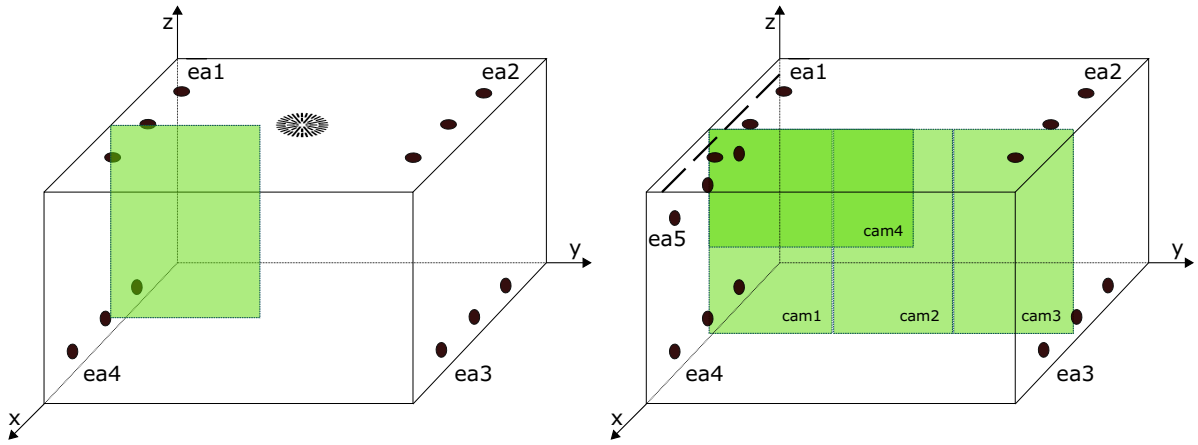

(a) swirl diffuser (b) slot diffuser

Figure 3: Tracked field of the light section by different camera positions for the two supply air cases

2.4 Numerical Model

The numerical CFD simulations are performed using the commercial software Simcenter Star-CCM+ v.2020.2[8]. Within this software, the creation of the geometry as a CAD model, the local discretization with a polyhedral mesh, determination of the boundary conditions and solver settings and the initial post-processing are carried out.

The investigated geometries base on the test stand. The inlets are imprints on the surface. The outlets are extended 0.3 m to prevent reversed flow. Swirl diffuser is simplified to a ring gap with an equivalent area.

A grid independancy study[9] is being conducted to find a mesh with low sensitivity on the distribution of the passive scalar in the room and best performance to reduce the computing costs (see Figure 4). The mesh has about 1.5 million cells. Even a coarser grid seems to satisfy. The wall boundary layers are resolved with the help of six prism layers. For the high velocities in the ceiling area, it is difficult to achieve a y^+ value less than or equal to 1 without increasing the cell number on a justifiable level. Therefore, an all y^+ wall-treatment is to be applied.

[8]Siemens Digital Industries Software

[9]The subsequent aim of the research project is to evaluate the ventilation effectiveness, therefore the age of the air is considered as a quality characteristic in the grid independancy study.

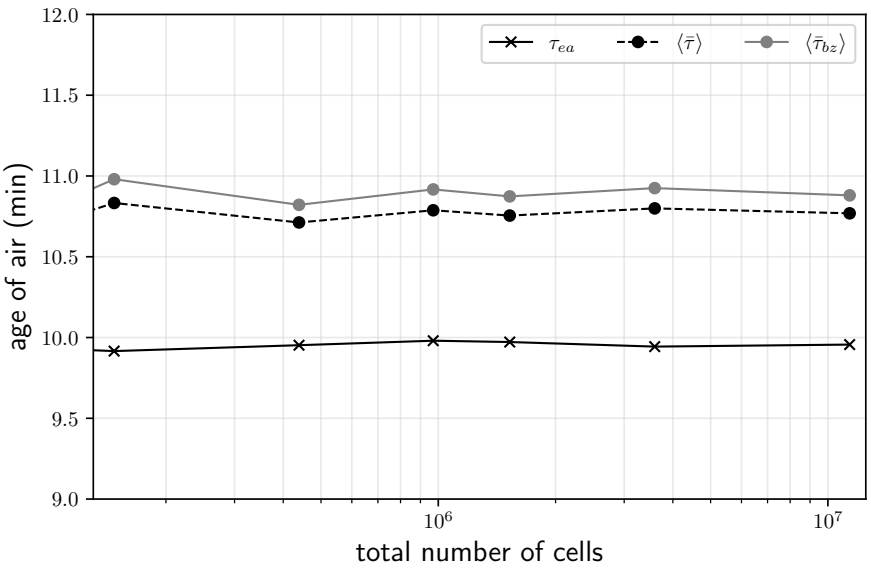

Figure 4: Mesh indipendency study: sensitivity of different age of air values (age of air at the exhaust τ_{ea}, mean age of air $\langle\bar{\tau}\rangle$ and mean age of air in the breathing zone $\langle\bar{\tau}_{bz}\rangle$) over different cell densities

Navier-Stokes equations are a system of second order nonlinear partial differential equations and include the momentum conservation equation, continuity equation and energy conservation equation. These equations describe the flow of fluids. STAR-CCM+ uses the finite volume method to discretise these equations. The entire flow domain is divided into control volumes (cells). In each cell, the conservation equations are solved in discrete form and the solutions are stored in the center of the cell. A direct solution of these equations is bound to a very fine temporal and spatial discretization. To reduce the computational effort, assumptions are made for the evolution of the turbulence. The best known approach are the Reynolds-averaged Navier–Stokes (RANS) turbulence models. Time and location dependent flow variables of the unsteady Navier-Stokes equations are decomposed into mean and fluctuation values. This results in turbulent (Reynolds) stress tensor with unknowns that can be solved using different approaches. STAR-CCM+ offers two solution approaches: eddy viscosity models and Reynolds Stress Transport (RST) models [17]. In this study, the eddy viscosity models: Spalart-Allmaras, k-ϵ realizable,

Table 5: Summary of mesh, boundary, and solver settings

mesh settings	1.5 mio. polyeder cells, 6 prism layer
turbulence model	RANS, Reynolds Stress Turbulence Model (Elliptic Blending) all y^+
radiation	Gray-Thermal-Radiation, Surface-to-surface radiation
solver	Segragated, 2nd order convection scheme
medium	ideal gas, gravity
supply air	Mass flow inlet (Q_{sa} = 100 or 400 $\mathrm{m^3\,h^{-1}}$, T_{sa} = 291.15 K)
exhaust air	Outlet
walls, ceiling, floor	adiabatic

k-ω SST and the RST model with elliptic blending are compared.

The eddy viscosity models assume a linear relationship between the strain-rate and the Reynolds-stress tensor (also known as Boussinesq assumption). The Spalart-Allmaras is simple, robust and need less computing power. It was developed for the computation of the aerodynamics of wings and therefore it is rather not suitable for the computation of space flows. For the calculation of space flows, the properties of the k-ϵ turbulence model are advantageous. There are numerous submodels for this. If it is not clear which turbulence model to use in a particular situation, the realizable two-layer k-ϵ model would be a reasonable choice [18, 19]. Also, the k-ω shear stress transport (SST) combines the advantages of the k-ω model in the near-wall region with the advantages of the k-ϵ model in free flow far from the wall.

A more accurate modeling of complex flows compared to the eddy viscosity models is possible with the RST models [20]. However, this also means a higher computational effort and additional storage space is necessary, because five additional equations has to be solved compared to a k-ϵ turbulence model. The RST models solve the Reynolds stress tensor from transport equations derived from the Navier-Stokes equations. This results in new unknowns: turbulent transport, dissipation and pressure strain. Depending on how the last unknown is modeled, different RST models result. The elliptic blending pressure-strain model offers an all y^+ wall-treatment which minor the convergence issues of RST models [21, 22].

All other chosen boundaries, models and settings are summarized in Table 5.

2.5 Comparison of the Airflow Characteristic

The airflow tracked from the PST-System is compared to the airflow in the simulation. Therefore an equidistant grid of 59 times 53 (59 times 104 for the slot diffuser) vectors is exported from the CFD and EFD data. First, the deviation of the alignment of the vector field is to be compared independently of the magnitude of the vectors. For this purpose the cosine theorem is applied [9, 10]. For each point in the grid the cosine of the angle α_i between the EFD $\vec{u}_{i,exp}$ and CFD vector $\vec{u}_{i,num}$ is determined (1). Finally, the mean value over all individual deviations is used as the overall measure for the similarity of the airflow (2).

$$\cos\alpha_i = \frac{\vec{u}_{i,exp} \cdot \vec{u}_{i,num}}{|\vec{u}_{i,exp}| \cdot |\vec{u}_{i,num}|} \tag{1}$$

$$\langle cos\alpha \rangle = \frac{1}{n} \sum_{i=1}^{n} \cos\alpha_i \tag{2}$$

The cosine-function is not linear. Thus, values from $\frac{\sqrt{2}}{2}$ to 1 and $-\frac{\sqrt{2}}{2}$ to -1 are more likely to be (see Figure 5a). Thus, a linearization is used to define the similarity value Sim' (3)). A value of one means the vector plots are identical and a value of zero means they are exactly opposite.

$$Sim' = 1 - \frac{1}{n\pi} \sum_{i=1}^{n} \arccos \frac{\vec{u}_{i,exp} \cdot \vec{u}_{i,num}}{|\vec{u}_{i,exp}| \cdot |\vec{u}_{i,num}|} \tag{3}$$

(a) cos α (b) Sim'

Figure 5: Similarity value for two vectors

Second, the deviation of the magnitude of the vectors is to be compared. The room averaged value used for the assessment is named similarity of the vector magnitudes Sim'' (4). A Sim''-Value of one means that the averaged velocity between experiment and simulation are equal. If it is greater than one the simulated velocity is greater than the experimental and if it is smaller than one the simulated velocity is below the experimental.

The data science and plots are carried out with the programming language Python[10] and the use of the libaries NumPy [23], Matplotlib [24], and Pillow[11].

$$Sim'' = \frac{1}{n} \sum_{i=1}^{n} \frac{|\vec{u}_{i,num}|}{|\vec{u}_{i,exp}|} \tag{4}$$

[10]Python Software Foundation
[11]Pillow is a PIL fork by Alex Clark and Contributors

3 Results

Regarding the similarity of the vector directions Sim' for the slot diffuser the average value is at 0.65 and for the swirl diffuser slightly lower at 0.57 (see Tables 6 and 7). The averaged similarity for all high air change rate cases is 0.77. For all small air change rate cases it ts 0.49.

Table 6: Comparison of the CFD and EFD Sim' and Sim''-Values for the isothermal slot diffuser

	ea1.i5	ea1.i3	ea2.i5	ea2.i3	ea3.i5	ea3.i3	ea4.i5	ea4.i3	ea5.i5	ea5.i3
Sim'	0.76	0.59	0.78	0.53	0.73	0.54	0.75	0.57	0.73	0.54
Sim''	1.07	0.55	1.29	1.05	0.98	1.07	1.00	1.06	1.07	0.91

Table 7: Comparison of the CFD and EFD Sim' and Sim''-Values for the isothermal swirl diffuser

	ea12.i5	ea12.i3	ea34.i5	ea34.i3
Sim'	0.80	0.31	0.82	0.33
Sim''	2.32	1.57	2.68	1.09

For the velocity magnitude distribution Sim'', there is an overestimation of the velocities in the simulation for high air changes and a good agreement for the smaller air change. For the slot diffuser the average value is at 1.01 and for swirl diffuser at 1.91. The high difference between slot and swirl diffuser can be explained by the insufficient tracking of the supply air jet velocities at the swirl diffuser. This amplifies the deviations between CFD and EFD data especially for higher flow rates. Reducing the comparison by the upper two rows of datapoints in which the supply air jet is dominand the Sim''-Value decrease by three to nine percent.

Besides the similarity values, vector plots show the airflow in the midsection of the room. This vector plots show for the CFD data the vector orientation and magnitude, not just the tangential velocity profile. In the simulations, the formation of a vortex for the lower air exchange remains stable. This cannot be validated by the PST measurements (see Figure 6 and 7).

For the swirl diffuser a strechtching of the vortex can be observed depending on the exhaust air position. The near-bottom exhaust position ea34 and ea4 compared to ea 12 and ea1 pull the vortex down (see Figure 7). This characteristic is to be considered in simulation and experiment.

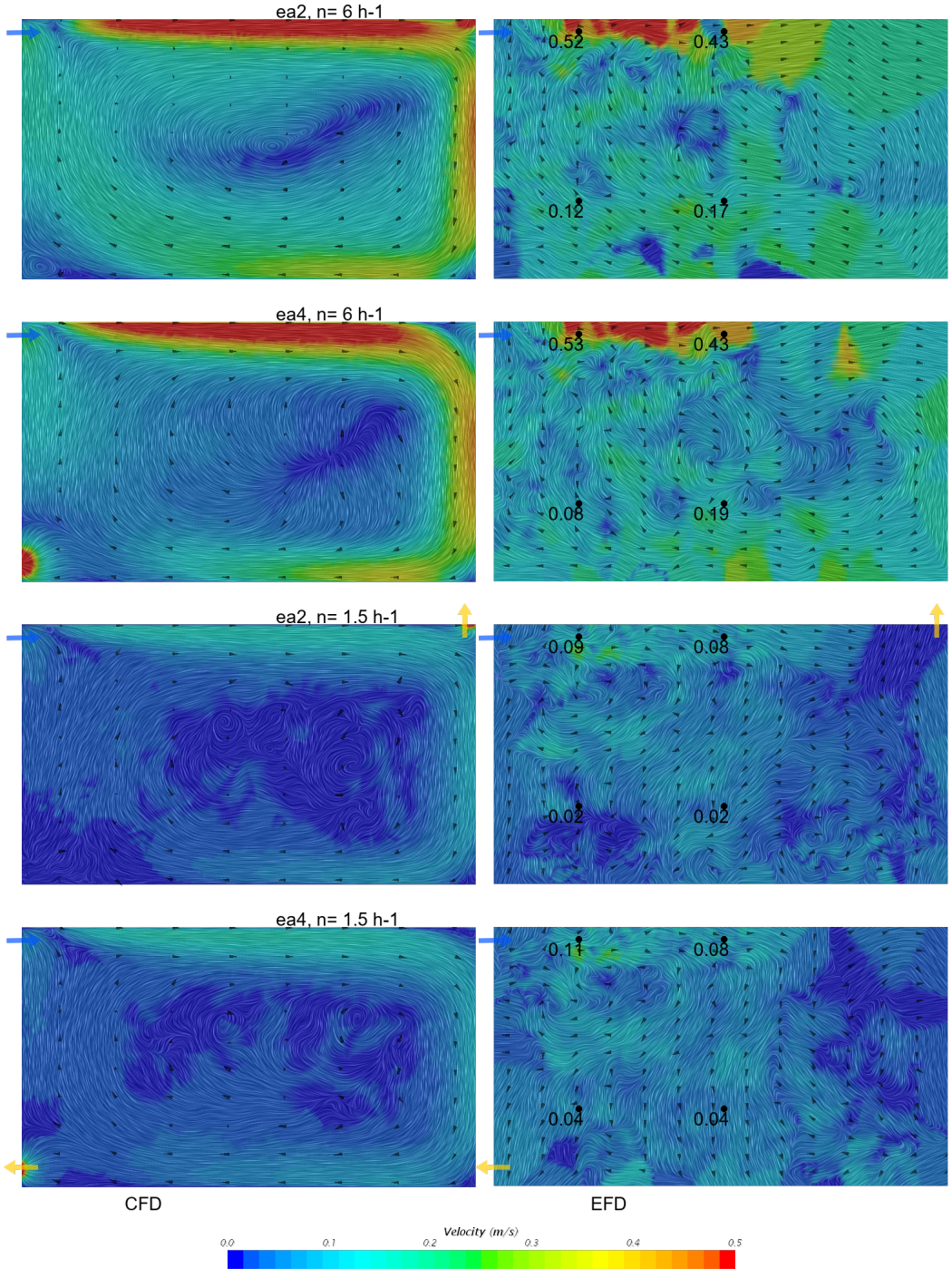

Figure 6: Comparison of the CFD and EFD vector plots for the isothermal slot diffuser. Black dots show the position of hotwire anemometer measured points with the average velocity magnitude in $\mathrm{m\,s^{-1}}$.

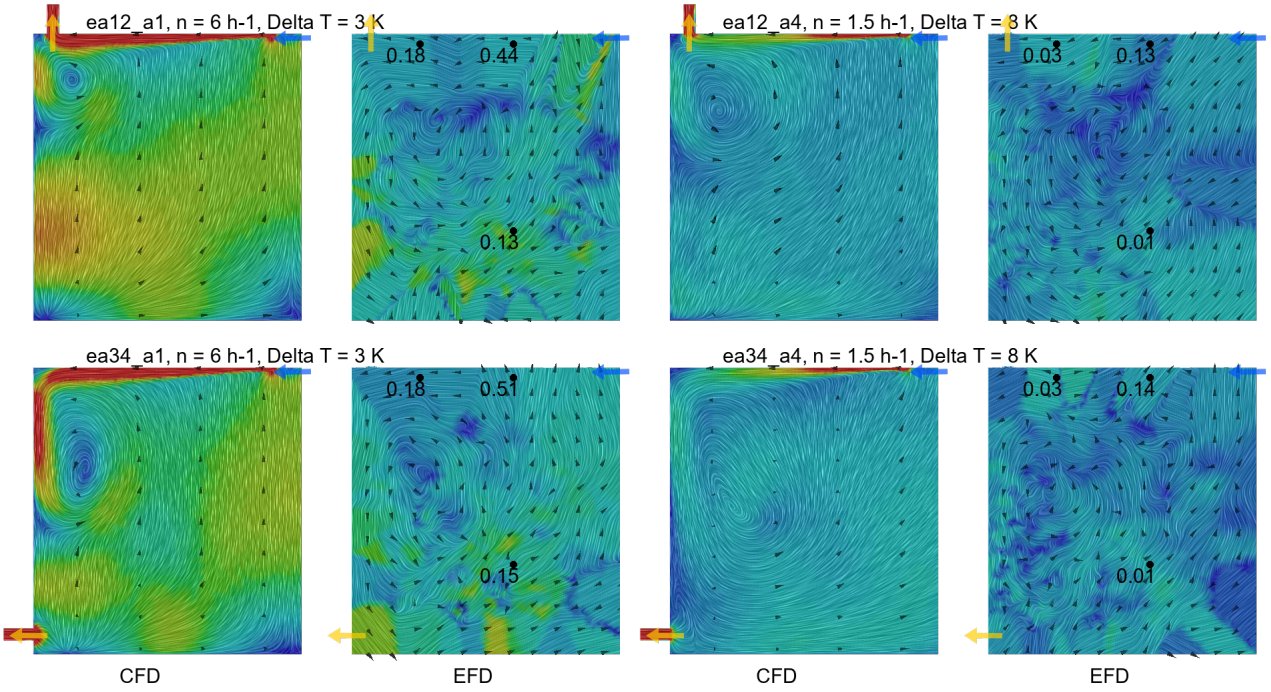

Figure 7: Comparison of the CFD and EFD vector plot for the isothermal swirl diffuser. Black dots show the position of hotwire anemometer measured points with the average velocity magnitude in $\mathrm{m\,s^{-1}}$.

3.1 Turbulence model

The simulations are mainly done with the RST elliptic blending turbulence model. For the swirl ea12 case, other RANS turbulence models are tested. The individual turbulence models show significant deviations from each other.

The best Sim'-Values are generated with the RST - and the k-ϵ realizable turbulence model between 0.8 and 0.82 (see Table 8). The k-ω SST and the Spalart-Allmaras turbulence model have lesser similarity value around 0.78. The bigger deviations are in the Sim''-Values. Here the RST model has the best value with 2.32. The value of the k-ϵ realizable turbulence model is 1.4 times higher for an air change rate of 6 h^{-1} and 1.2 times higher for an air change rate of 1.5 h^{-1}. Also, the k-ω SST turbulence model and the Spalart-Allmaras show higher velocity distributions.

Table 8: Comparison of the CFD and EFD Sim' and Sim''-Values for the isothermal swirl diffuser, the ceiling exhaust position ea12 and an air change rate $n = 6$ h^{-1} simulated with different turbulence models. In parentheses are values for the lower air change rate $n = 1.5$ h^{-1}

turbulence model	RST eliptic	k-ϵ realizable	k-ω SST	Spalart-Allmaras
Sim'	0.80 (0.31)	0.82 (0.30)	0.78	0.78
Sim''	2.32 (1.57)	3.34 (1.88)	2.93	3.15

The small differences in the Sim'-value suggest no visible differences. Figure 8 reveals visibly the deviation of the turbulence models from the EFD vector plot. The position and form of the characterisic vortex shifts for the k-ω SST and the Spalart-Allmarass turbulence models.

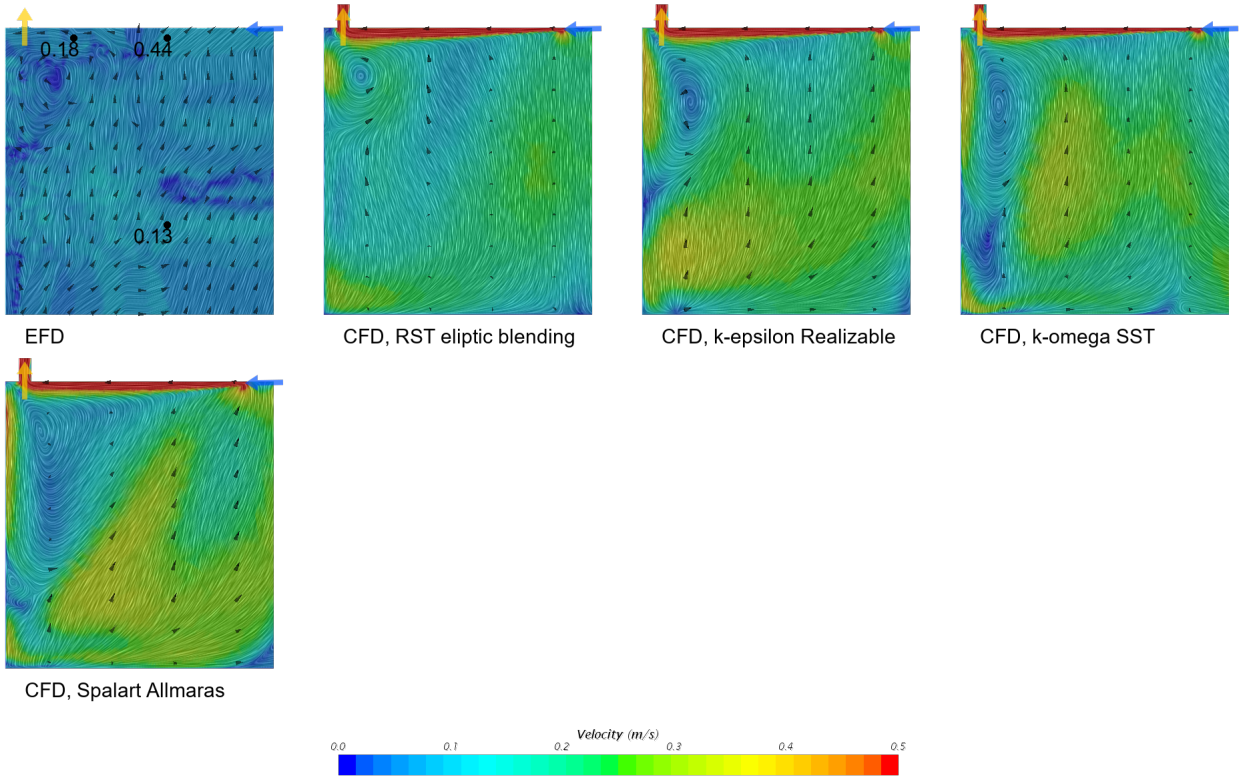

Figure 8: Comparison of the CFD and EFD vector plots for the isothermal swirl diffuser, the ceiling exhaust position ea12 and an air change rate $n = 6\ \mathrm{h}^{-1}$ simulated with different turbulence models. Black dots show the position of hotwire anemometer measured points with the average velocity magnitude in $\mathrm{m\,s}^{-1}$.

3.2 Sensititvity supply air inlet

The swirl diffuser is simplified to a ring gap. Thus, an input uncertainty is the result. The gap space should be equivalent to the open space of the swirl diffuser in the test stand. Regarding the measurements, in particular the hot-wire anemometry measure points, it becomes obvious that the momentum of the supply air jet is overrated by the simulation. To reduce the momentum, the gap size is widened. The original gap area is 0.021 m^2. In a first step it is widened to 0.045 m^2 and in a second to 0.068 m^2.

The gap widening has an effect on the Sim'-value (see Table 9). Doubling the ring gap rise the Sim'-value by 5 % and tripling the ring gap rise the Sim'-value by 1 %. Thus, the numerical solution approximates the experimental best, by reducing the supply air momentum with an ring gap area 0.045 m^2.

Table 9: Comparison of the CFD and EFD Sim' and Sim''-Values for the isothermal swirl diffuser, the ceiling exhaust position ea12 and an air change rate $n = 6$ h^{-1} simulated with different ring gap sizes for the swirl diffuser

A_{sa} (m^2)	0.021	0.045	0.068
Sim'	0.8	0.84	0.81
Sim''	2.32	1.88	1.79

Sim''-value shows a reduction for the ring gap with 0.045 m^2 and 0.068 m^2. Additionally, regarding Figure 9 there is a visible velocity reduction, which fits much better the experimental results.

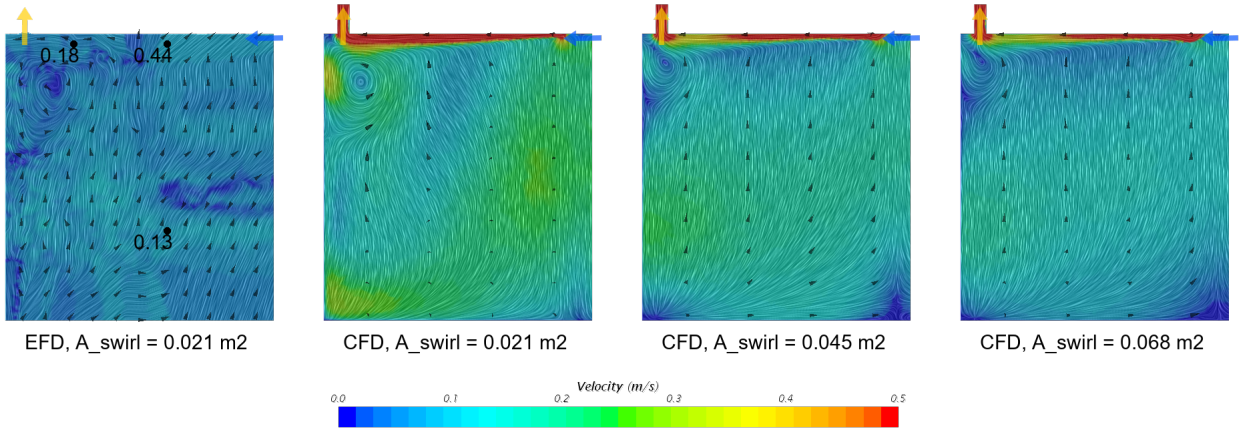

Figure 9: Comparison of the CFD and EFD vector plots for the isothermal swirl diffuser, the ceiling exhaust position ea12 and an air change rate $n = 6$ h^{-1} simulated with different ring gap sizes for the swirl diffuser. Black dots show the position of hotwire anemometer measured points with the average velocity magnitude in m s^{-1}.

3.3 Sensititvity exhaust diameter

The exhaust air diffuser in the test stand is not just an open duct as modeled in the CFD simulation. A poppet ventil is attached to regulate manually the pressure resistance. To validate the effects of a higher and lower resistance, the exhaust diameter is alternated. The original value is 0.125 m, which is decreased to 0.06 m and increased to 0.282 m.

The similarity of the airflow is negligible for the lower diameter as the higher diameter (see Table 10). A reduction of the exhaust diameter has a significant influence raising the

Sim''-value by 42 %. The reduction especially effects the velocity speed and direction in the lower part (see Figure 10). A widening of the exhaust opening reduces the Sim''-value by only 2 %.

Table 10: Comparison of the CFD and EFD Sim' and Sim''-Values for the isothermal swirl diffuser, the ceiling exhaust position ea12 and an air change rate $n = 6\ \mathrm{h}^{-1}$ simulated with different exhaust diameters

d_{ea} (m)	0.06	0.125	0.282
Sim'	0.17	0.2	0.16
Sim''	3.29	2.32	2.28

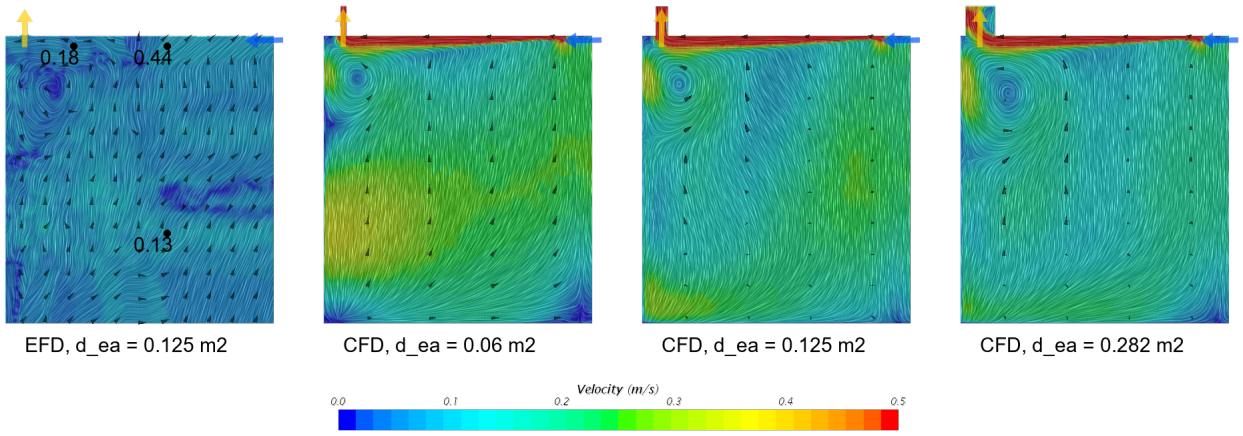

Figure 10: Comparison of the CFD and EFD vector plots for the isothermal swirl diffuser, the ceiling exhaust position ea12 and an air change rate $n = 6\ \mathrm{h}^{-1}$ simulated with different exhaust diameters. Black dots show the position of hotwire anemometer measured points with the average velocity magnitude in $\mathrm{m\,s}^{-1}$.

4 Discussion

The agreement of the flow between simulation and experiment is high for a high momentum. For the smaller air change rate, the flow velocities decrease. With decreasing flow velocities, the accuracy of the PST system also decreases. On the one hand, the influence of the helium-air mixture increases if exact density neutrality is not achieved and, on the other hand, the soap bubbles have an intrinsic momentum when leaving the diffuser outlet. This self-momentum disturbs the flow in the area of the light cut. Since the bubbles have only a limited dwell time. Recordings with a thermal imaging camera (testo 868) have shown that the isothermal boundary conditions cannot be maintained so well in the experiment for the small supply air volume flow. The wall temperature fluctuates between 19.2 and 20 °C. The supply air stream heats up to 20.6 K. Here, too, the influences are amplified: higher temperature difference and lower free-jet momentum, so that the flow pattern in the experiment is disturbed. These disturbances affect the airflow of the experiment hereditarily for small air exchange rates, so that there is no agreement with a disturbance-free simulation.

The structure of the flows has a higher stability in the simulation. On the one hand, this is due to the fact that all disturbance effects can be excluded, but above all it is due to a higher momentum of the supply air jet. The annular gap was modeled in the simulation with the effective supply air opening of the swirl diffuser according to the manufacturer's specifications. The effective supply air opening is defined by the air control elements in the swirl diffuser and not with the actual free area. A re-measurement of the free area planar with the ceiling results in 0.048 m^2. As the sensitivity analysis has shown, the velocities of experiment and simulation then increasingly converge.

Using the cosine theorem as a similarity value method is quick and straightforward. A danger is that two flows have the same features (e.g. vortices), but these are displaced and thus are not evaluated as similar. This could be the reason that the agreement

of the airflow (Sim') for the high air change rate between experiment and simulation is higher for the swirl diffuser than for the slot diffuser. Although qualitatively there is a good match in both cases. Another reason could be the stability of the airflow structure. The stability of the simulated airflow is higher than for the experimental one. Kandzia used the Archimedes number to evaluate the stability of flow structures [2]. The Archimedes number Ar, expresses whether the flow is dominated by buoyancy forces or by friction forces. Falling below the stability limit results in changing the airflow structure by the exhaust position. In this study there are only isothermal cases, but the parameter study will take unisothermal cases as well. Thus, a flow structure evaluation has to be taken into account in future investigations and the similarity-value may help to define a threshold-level.

The similarity value Sim'' has higher deviations as Sim'. Comparing huge areas of vectors needs a sufficient data density. Tracking all velocity levels experimentally requires an adaption of the camera settings. So higher velocities like the supply air jet for the swirl diffuser are not taken into account and the deviation rise. Additionally, the velocity normal to the section could not be tracked with the PST-System. Thus, only tangential velocities are comparable between CFD and EFD.

RST turbulence models have low acceptance [20] due to their higher computational complexity, lower dissemination, and higher susceptibility to errors. The most widely used turbulence model is the k-ϵ turbulence model with its various submodels. These usually produce good results for room airflow simulations [25, 26]. The RST model has advantages for flows with streamline curvatures. Thus, a swirling flow is better modeled [27]. To make the differences between the k-ϵ realizable and RST model visible, the velocity is plotted normally to the section view in Figure 11. The twist is much more pronounced in the RST. This reduces the velocities tangential to the section plane. As a result, the RST model more closely approximates the experimental solution than the k-ϵ realizable. That the simulated velocity for fully developed turbulence regions is higher with the k-ϵ realizable than with the k-ω SST is also observed in [28].

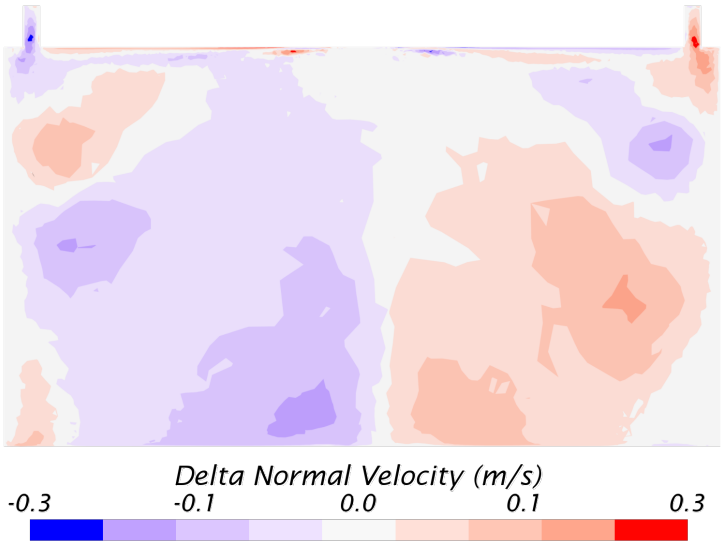

Figure 11: Difference of velocity normal to the section between the simulation with RST turbulence model and k-ϵ realizable turbulence model (the ceiling exhaust position ea12 and an air change rate $n = 6$ h^{-1})

The solver time on an average PC i5-7500 CPU is 28.14 seconds per iteration for the RST turbulence model and 14.84 seconds per iteration for the k-ϵ realizable. To converge the residuals the RST-Model needs two times more iterations than the k-ϵ realizable. Thus, the RST simulation takes four times longer to calculate.

5 Conclusion

This study compares the airflow measured and simulated in a moderate room with an area of 23 m^2. The measurements are taken with a PST-System in one section plane through the room. Flow velocities are overestimated in the simulation especially for the swirl diffuser. The difference can be partly explained by the insufficient recording of the velocities of the supply air jet. However, the influences of geometric model errors are much more likely. The most obvious error is the simplification of the supply air diffuser geometry to a ring gap. An increase of the ring gap reduces the supply air impulse and also the velocities in the occupied zone.

Even though the velocities are not directly comparable without adjusting the ring gap, there is a good agreement in the flow structure. The flow structure influences the convective transport routes and thus decisively determines the ventilation effectiveness. Therefore, the simulations can be considered valid. For small air changes, however, this must be limited, since it must be assumed that room airflows are always subject to disturbance variables and conclusions from a simulation are not transferable.

An exciting observation is the experimental and numerical visualization of the vortex stretching with the swirl diffuser. With an exhaust position near to the floor, the vortex will be stretched downwards. This is confirme small changes of the airflow in the room. A quantification of the influence of the exhaust positioning should be worked out with the parameter study.

The RST turbulence model with elliptic blending shows excellent properties in this study and the additional computing effort is nowadays easy to accept. Hopefully, it will be considered more often in future investigations to validate a general performance in indoor air simulations.

Acknowledgments

The project described in this article was funded by the German Federal Ministry for Economic Affairs and Energy (BMWi) under the IGF funding code 20440 N. The authors assume responsibility for the content of this publication

References

[1] Bernd M. Hanel, Markus Rösler, and Götz Morgenstern. *Raumluftströmung*. 2. durchgesehene Aufl. Huethig: C.F. Müller Verlag, 1996. ISBN: 3788075570.

[2] Claudia Kandzia. *Experimentelle Untersuchung der Strömungsstrukturen in einer Mischlüftung: Aachen, Techn. Hochsch., Diss., 2013*. Vol. 20. E.ON Energy Research Center / EBC - Energy Efficient Buildings and Indoor Climate. Aachen: Hochschulbibliothek der Rheinisch-Westfälischen Technischen Hochschule Aachen, 2014. ISBN: 9783942789196. URL: http://nbn-resolving.de/urn:nbn:de:hbz:82-opus-49811.

[3] P. V. Nielsen, Chen Zhang, A. Bugenings, and M. Schaffer. "THE DEVELOPMENT OF A BENCHMARK FOR ROOM AIR DISTRIBUTION: THE BACKWARD FACING STEP FLOW". In: *RoomVent 2020* (2021).

[4] ASME. *Standard for verification and validation in computational fluid dynamics and heat transfer: An American national standard*. Reaffirmed 2016. Vol. 20-2009. ASME V&V. New York, NY: The American Society of Mechanical Engineers, 2009. ISBN: 9780791832097.

[5] Qingyan Chen and J. Srebric. "A Procedure for Verification, Validation, and Reporting of Indoor Environment CFD Analyses". In: *HVAC&R Research* 8.2 (2002), pp. 201–216. ISSN: 1078-9669. DOI: 10.1080/10789669.2002.10391437.

[6] Hugh W. Coleman and W. Glenn Steele. *Experimentation, validation, and uncertainty analysis for engineers*. Fourth edition. Hoboken, NJ, USA: John Wiley & Sons Inc, 2018. ISBN: 111941766X. DOI: 10.1002/9781119417989. URL: https://onlinelibrary.wiley.com/doi/book/10.1002/9781119417989.

[7] Dirk Müller. "Optische Erfassung und numerische Berechnung von 2- und 3-Dimensionalen Geschwindigkeitsfeldern mit niedrigen turbulenten Reynoldszahlen". PhD thesis. 2000.

[8] William L. Oberkampf and Matthew F. Barone. "Measures of agreement between computation and experiment: Validation metrics". In: *Journal of Computational Physics* 217.1 (2006), pp. 5–36. ISSN: 00219991. DOI: 10.1016/j.jcp.2006.03.037.

[9] William P. Jones and George W. Furnas. "Pictures of relevance: A geometric analysis of similarity measures". In: *Journal of the American Society for Information Science* 38.6 (1987), pp. 420–442. ISSN: 0002-8231. DOI: 10.1002/(SICI)1097-4571(198711)38:6{\textless}420::AID-ASI3{\textgreater}3.0.CO;2-S.

[10] Ingo Schmitt. *Ähnlichkeitssuche in Multimedia-Datenbanken: Retrieval, Suchalgorithmen und Anfragebehandlung: Zugl.: Magdeburg, Univ., Fak. für Informatik, Habil.-Schr., 2004*. München: Oldenbourg, 2006. ISBN: 3-486-57907-X.

[11] H. K. Versteeg and W. Malalasekera. *An introduction to computational fluid dynamics: The finite volume method*. 2nd ed. Harlow England and New York: Pearson Education Ltd, 2007. ISBN: 9780131274983.

[12] Patrick J. Roache. “Verification of Codes and Calculations”. In: *AIAA Journal* 36.5 (1998), pp. 696–702. ISSN: 0001-1452. DOI: 10.2514/2.457.

[13] Claudia Balasus. *Entwicklung und Betrieb einer mobilen Teilklimaanlage, Messung und Auswertung von Temperaturphasenverläufen*. 2007.

[14] D. Müller and U. Renz. “A Low Cost Particle Streak Tracking System (PST) and a New Approach to Three Dimensional Airflow Velocity Measurements”. In: *RoomVent 1998* (1998).

[15] D. Müller and U. Renz. “A Particle Streak Tracking System (PST) to Measure Flow Fields in Ventilated Rooms”. In: *RoomVent 2020* (2000).

[16] R. Rank. *Untersuchung verschiedener Blasenflüssigkeiten zur Verwendng mit einem Helium-Blasengenerator zur Sichtbarmachung von Raumluftströmungen*. 2005.

[17] Siemens Digital Industries Software. *Support Center: Wissensdatenbank für Simcenter STAR-CCM+*. Ed. by Siemens Digital Industries Software. URL: https://support.sw.siemens.com.

[18] Tsan-Hsing Shih, William W. Liou, Aamir Shabbir, Zhigang Yang, and Jiang Zhu. “A new k-epsilon eddy viscosity model for high reynolds number turbulent flows”. In: *Computers & Fluids* 24.3 (1995), pp. 227–238. ISSN: 00457930. DOI: 10.1016/0045-7930(94)00032-T.

[19] P. L. Davis, A. T. Rinehimer, and M. Uddin. “A Comparison of RANS-Based Turbulence Modeling for Flow over a Wall-Mounted Square Cylinder”. In: *20th Annual Conference of the CFD Society of Canada* (2012).

[20] Q. Chen. “Prediction of room air motion by Reynolds-stress models”. In: *Building and Environment* 31.3 (1996), pp. 233–244. ISSN: 03601323. DOI: 10.1016/0360-1323(95)00049-6.

[21] R. Manceau and K. Hanjalić. “Elliptic blending model: A new near-wall Reynolds-stress turbulence closure”. In: *Physics of Fluids* 14.2 (2002), pp. 744–754. ISSN: 1070-6631. DOI: 10.1063/1.1432693.

[22] S. Lardeau and R. Manceau. “Computations of complex flow configurations using a modified elliptic-blending Reynolds-Stress model”. In: *HAL* (2016). URL: https://hal.archives-ouvertes.fr/hal-01051799.

[23] Charles R. Harris, K. Jarrod Millman, Stéfan J. van der Walt, Ralf Gommers, Pauli Virtanen, David Cournapeau, Eric Wieser, Julian Taylor, Sebastian Berg, Nathaniel J. Smith, Robert Kern, Matti Picus, Stephan Hoyer, Marten H. van Kerkwijk, Matthew Brett, Allan Haldane, Jaime Fernández Del Río, Mark Wiebe, Pearu Peterson, Pierre Gérard-Marchant, Kevin Sheppard, Tyler Reddy, Warren Weckesser, Hameer Abbasi, Christoph Gohlke, and Travis E. Oliphant. “Array programming with NumPy”. In: *Nature* 585.7825 (2020), pp. 357–362. DOI: 10.1038/s41586-020-2649-2.

[24] John D. Hunter. “Matplotlib: A 2D Graphics Environment”. In: *Computing in Science & Engineering* 9.3 (2007), pp. 90–95. ISSN: 1521-9615. DOI: 10.1109/MCSE.2007.55.

[25] Q. Chen. “COMPARISON OF DIFFERENT k-epsilon MODELS FOR INDOOR AIR FLOW COMPUTATIONS”. In: *Numerical Heat Transfer, Part B: Fundamentals* 28.3 (1995), pp. 353–369. ISSN: 1040-7790. DOI: 10.1080/10407799508928838.

[26] P. V. Nielsen. “The Selection of Turbulence Models for Prediction of Room Airflow”. In: *ASHRAE Transactions* 104 part 1B (1998), pp. 1119–1127.

[27] Joel H. Ferziger and Milovan Peric. *Numerische Strömungsmechanik*. Berlin, Heidelberg: Springer Berlin Heidelberg, 2008. ISBN: 978-3-540-67586-0. DOI: 10.1007/978-3-540-68228-8.

[28] Jia-Wei Han, Wen-Ying Zhu, and Zeng-Tao Ji. “Comparison of veracity and application of different CFD turbulence models for refrigerated transport”. In: *Artificial Intelligence in Agriculture* 3 (2019), pp. 11–17. ISSN: 25897217. DOI: 10.1016/j.aiia.2019.10.001.